Electronic Supplementary Material (ESI) for Nanoscale.

InSe:Ge-Doped InSe van der Waals Heterostructure to Enhance Photogenerated Carrier Separation for Self-Powered Photoelectrochemical-Type Photodetector

Liping Liao, [a,*] *Bing Wu,* [a] *Evgeniya Kovalska,* [a] *Filipa M. Oliveira,* [a] *Jalal Azadmanjiri,* [a] *Vlastimil Mazánek,* [a] *Lukáš Valdman,* [a] *Lucie Spejchalová,* [a] *Cunyun Xu,* [b] *Petr Levinský,* [c] *Jiří Hejtmánek,* [c] *Zdeněk Sofer* [a *]

[a] Department of Inorganic Chemistry, University of Chemistry and Technology Prague, Technická 5, 166 28 Prague 6, Czech Republic

[b] Institute for Clean Energy and Advanced Materials, School of Materials and Energy, Southwest University, Chongqing Key Laboratory for Advanced Materials and Technologies of Clean Energy, Chongqing 400715, P. R. China

[c] FZU - Institute of Physics of the Czech Academy of Sciences, Cukrovarnická 10/112, 162 00 Prague 6, Czech Republic

E-mail: soferz@vscht.cz ; liaol@vscht.cz

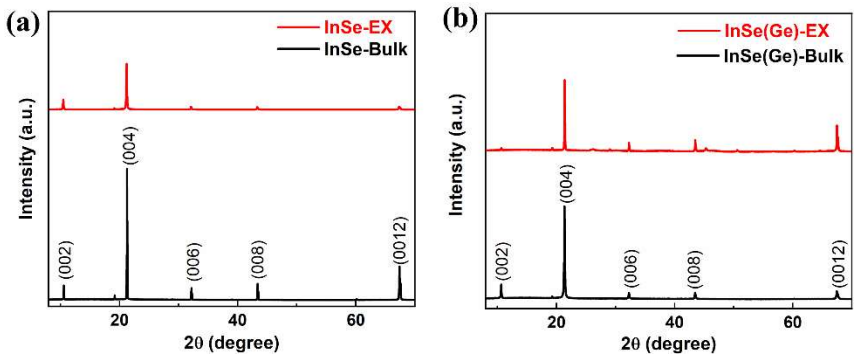

Fig. S1. XRD patterns of bulk and exfoliated samples: (a) InSe; (b) InSe(Ge).

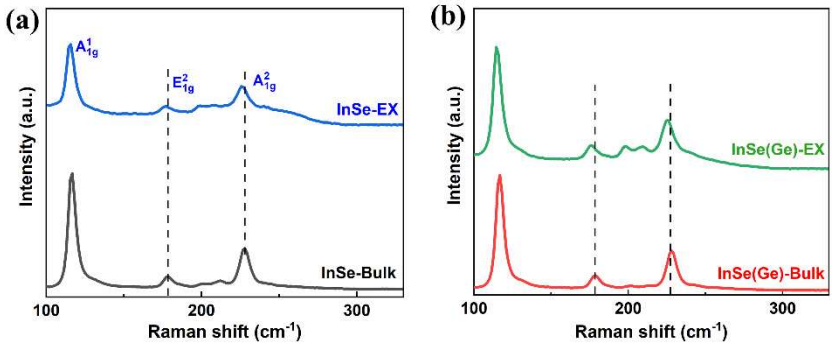

Fig. S2. The Raman spectra of bulk and exfoliated samples: (a) InSe; (b) InSe(Ge).

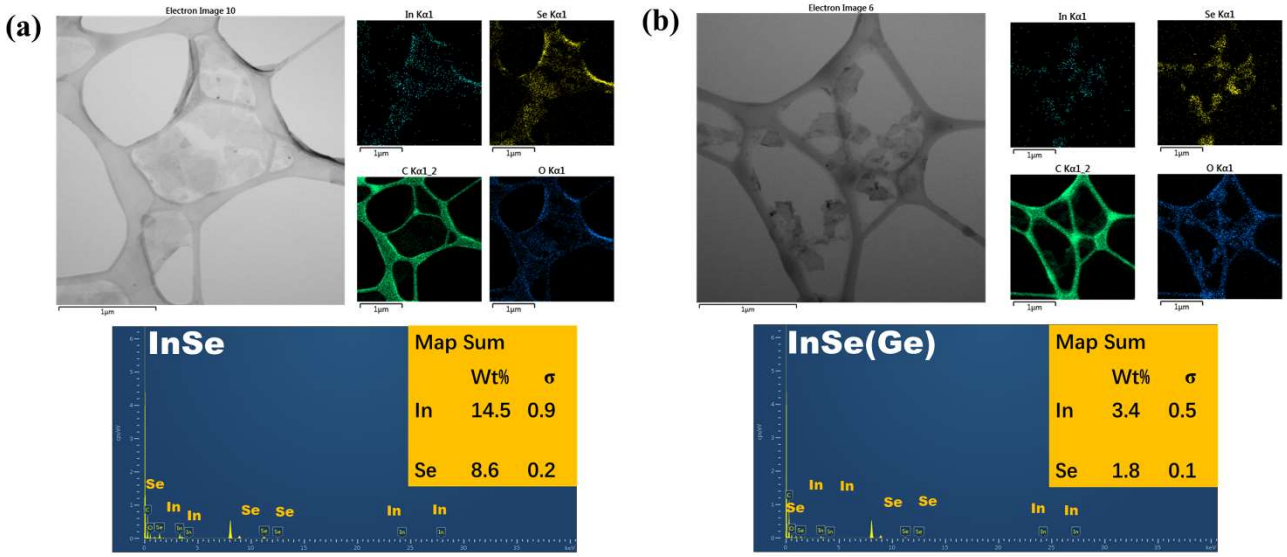

Fig. S3. TEM images, and corresponding EDS mapping images of (a) Exfoliated InSe and corresponding EDS spectra, (b) Exfoliated InSe(Ge) and corresponding EDS spectra.

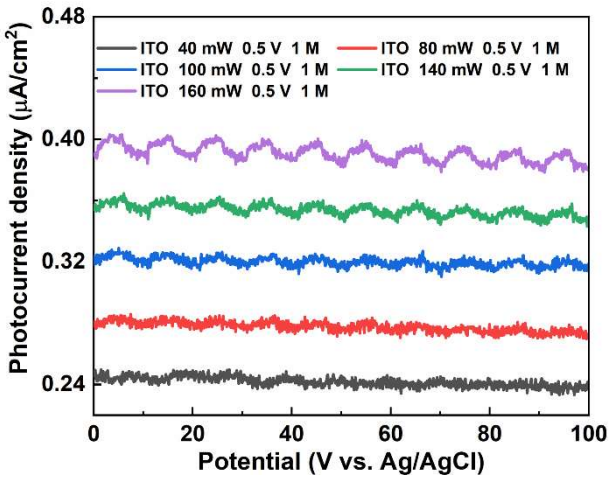

Fig. S4. PEC transient photoresponse of bare ITO under the illumination intensity of 160 mW cm^{-2} (blue LED, ~460 nm) in 1 M KOH.

Table S1. Time response paraments of InSe, InSe(Ge), and InSe/InSe(Ge) heterostructure in 0.1 M, 0.5 M, and 1 M KOH electrolytes at 0.5 V bias.

Device	**KOH concentration**		
	0.1 M	**0.5 M**	**1 M**
	t_r/t_f	t_r/t_f	t_r/t_f
InSe	0.65s/0.8s	0.5s/0.8s	0.25s/0.35s
InSe(Ge)	0.9s/1.5s	0.92s/1s	0.5s/0.65s
Heterostructure	0.188s/0.3s	0.138s/0.16s	0.128s/0.1s

Table S2. Time response paraments of InSe, InSe(Ge), and InSe/InSe(Ge) heterostructure in 0.1 M, 0.5 M, and 1 M KOH electrolytes at 0 V bias.

Device	**KOH concentration**		
	0.1 M	**0.5 M**	**1 M**
	t_r/t_f	t_r/t_f	t_r/t_f
InSe	0.4s/0.45s	0.25s/0.38s	0.13s/0.185s
InSe(Ge)	0.6s/1s	0.45s/0.55s	0.2s/0.28s
Heterostructure	0.15s/0.2s	0.102s/0.15s	0.095s/0.091s

Table S3. Detectivity, EQE of InSe, InSe(Ge) and InSe/InSe(Ge) heterostructure at 0.5 V applied bias potential and in 0.5 M KOH.

	Detectivity(Jones)			**EQE**		
Power density ($mWcm^{-2}$)	Heterostructure	InSe	InSe(Ge)	Heterostructure	InSe	InSe(Ge)
40	3.08×10^{11}	4.07×10^{10}	1.96×10^{9}	21.2%	2.8%	0.13%
80	2.28×10^{11}	4.26×10^{9}	1.95×10^{9}	15.7%	2.9%	0.13%
120	2.01×10^{11}	3.73×10^{10}	2×10^{9}	13.8%	2.5%	0.12%
140	1.67×10^{11}	3.7×10^{10}	1.33×10^{9}	11.6%	2.5%	0.09%
160	1.08×10^{11}	3.6×10^{10}	1.3×10^{9}	7.4%	2.4%	0.09%

Table S4. Performance comparison of the self-powered photodetectors based on 2D materials.

Configuration type	Materials	Measurement conditions	Responsivity	Response time	Refs.
p-n Junction photodetectors	p-WSe_2/n-MoS_2	532 nm	10 mA W^{-2}	1 µs	4
	p-GaSe/n-InSe	470 nm	21 mA W^{-1}	2 µs	5
	p-$MoTe_2$/n-MoS_2	410 nm	38 mA W^{-1}	NA	6
	p-MoS_2/n-WS_2	532 nm	4.36 mA W^{-1}	4 ms	7
	p-WSe_2/n-WS_2	514 nm	40 mA W^{-1}	100 µs	8
Schottky junction photodetectors	Au–InSe/Au–In	365 nm	369 mA W^{-1}	23 ms	9
	Au-BN/plasma Schottky contact	250 nm	296 mA W^{-1}	400 ms	10
	Graphene/Si	532 nm	510 mA W^{-1}	130 µs	11
	UCNPs/graphene/GaAs	980 nm	5.97 mA W^{-1}	40 ms	12
PEC-type photodetectors	Few-layers BP	Simulated sunlight 0.1 M KOH	2.65 mA W^{-1}	0.5 s	13
	2D Bi nanosheets	Simulated sunlight, 1 M NaOH	0.152 mA W^{-1}	NA	14
	MoS_2/graphene	Simulated sunlight, 0.5 M Na_2SO_4	NA	NA	15
	SnS_2/graphene	Simulated sunlight, solid electrolyte	90 nA W^{-1}	NA	16
	WS_2/TiO_2	Simulated sunlight, 0.5 M Na_2SO_4	0.35 mA W^{-1}	NA	17
	InSe/InSe(Ge)	460 nm 1 M KOH	78 µA W^{-1}	0.128 s	This work

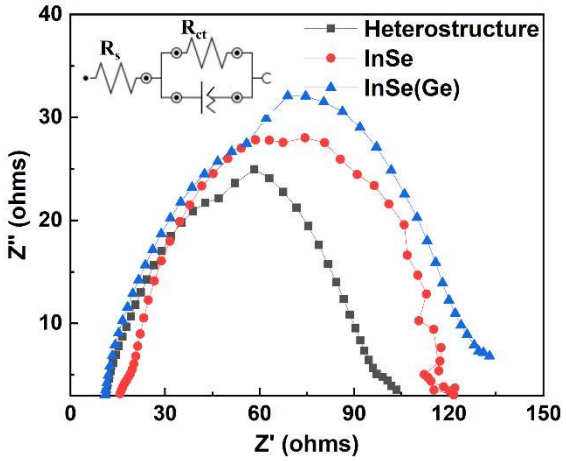

Fig. S5. Electrochemical impedance spectroscopy plots of InSe, InSe(Ge) and InSe/InSe(Ge) heterostructure in the frequency range of 0.01 Hz - 100 kHz under illumination (1 M KOH; blue LED: 160 mW cm^{-2}); Inset: Equivalent circuit.

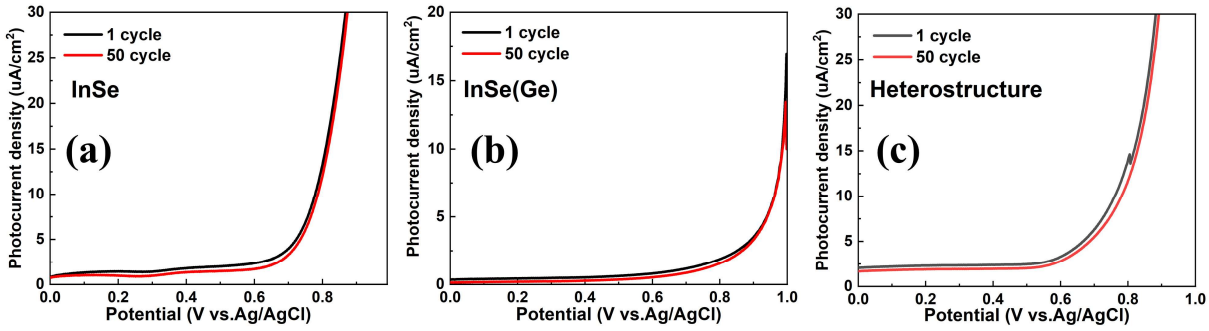

Fig. S6. LSV cycle stability test of pure InSe, pure InSe(Ge) and InSe/InSe(Ge) heterostructure in 1 M KOH.

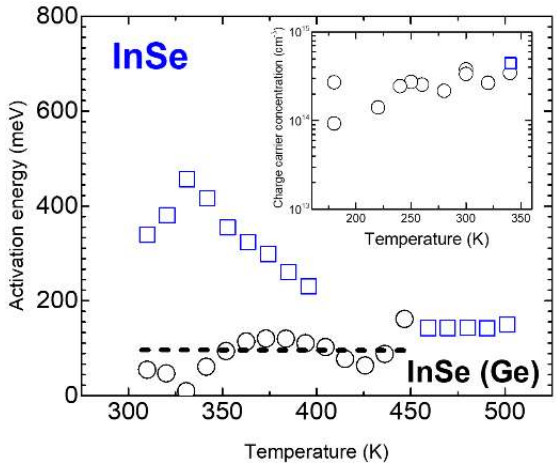

Fig. S7. Temperature dependence of the local activation energy of the electrical resistivity for InSe and InSe(Ge) crystals.

Supplementary note for Hall experiment analysis. For pristine crystal, the mobility was determined only at 340 K where the resistance of the sample enabled the Hall measurement. Here we summarize the peculiar observation consisting of (i) decreasing electron mobility with decreasing temperature for Ge doped sample; (ii) lower electron mobility of pure pristine InSe then doped sample; (iii) the activation energy of the electrical resistivity decreasing with increasing temperature for pristine InSe (Fig. S7) confronted with temperature-independent activation energy of Ge doped sample which exhibits, however, higher mobility, and (iv) extremely low carrier concentration detected by Hall measurement inevitably evoke the scenario where acceptors and donors mutually compensate.

Most concretely being framed by the high chemical purity (below ppm contamination of used

constituent elements In and Se), we should consider the role of native defects on the formation of donor/acceptor centers in InSe. The inspiration can be taken from the papers of D. Wang et al.[1] and H. Wang[2] where authors theoretically analyzed the formation and ionization energies of the native defects and substitutional impurities in mono- and few-layer InSe. Most importantly, the authors claim that selenium vacancy V_{Se} is formed relatively easily and represents the electrically neutral defect, while In vacancy V_{In} is a deep acceptor with high formation energy. Indium interstitial atom Inad stands, on the other hand, likely for the *n*-type conductivity like donor center in "pure" InSe and, considering the low doping level induced by Ge doping, also in Ge doped specimens.

Ge doped sample exhibits temperature-independent value of ~ 0.1 eV close to previously reported 0.09 eV.[3] In the inset, we depict the temperature dependence of the carrier concentration. In this respect, we presume that Se vacancy, which has the lowest formation enthalpy and is likely relatively abundant and electrically neutral defect, should be responsible for both the relatively low and mildly temperature-activated mobility. Considering the theoretical temperature-independent evolution in the case of "pure" neutral impurity scattering, we might accept that electron mobility observed in doped InSe(Ge) samples follows the temperature evolution typical for "ionized impurity scattering" the scenario of charged impurities takes place. Taking into account extremely low concentration of mobile electrons detected by Hall experiment ($n \sim 10^{14}$ cm^{-3}) we should then reconsider the effect of "charge compensation" of In vacancy (deep acceptor) and In interstitial (donor), which in combination not providing mobile charge carriers can be, however, responsible for temperature activated dynamics of electron scattering leading thus already below 350 K to $\sim T^{3/2}$.

Considering the Ge doping, let us note that a part of Ge species introduced into the initial melt can form a layered Ge-Se phase, contrary to the aimed In, Ge substitution in InSe. The minute

concentration of Ge-Se phase can be hardly discerned considering the analyzed Ge concentration of ~ 60 ppm in the sample InSe(Ge).

REFERENCES

1. Wang, D.; Li, X.-B.; Sun, H.-B., Native defects and substitutional impurities in two-dimensional monolayer InSe. *Nanoscale* **2017**, *9* (32), 11619-11624.
2. Wang, H.; Shi, J.-j.; Huang, P.; Ding, Y.-m.; Wu, M.; Cen, Y.-l.; Yu, T., Origin of n-type conductivity in two-dimensional InSe: In atoms from surface adsorption and van der Waals gap. *Physica E: Low-dimensional Systems and Nanostructures* **2018**, *98*, 66-73.
3. Shigetomi, S.; Ikari, T., Impurity levels in layered semiconductor n-InSe doped with Ge. *physica status solidi (b)* **2003**, *236* (1), 135-142.
4. 1.Lee, C.-H.; Lee, G.-H.; van der Zande, A. M.; Chen, W.; Li, Y.; Han, M.; Cui, X.; Arefe, G.; Nuckolls, C.; Heinz, T. F.; Guo, J.; Hone, J.; Kim, P., Atomically thin p-n junctions with van der Waals heterointerfaces. Nature Nanotechnology **2014**, 9 (9), 676-681.
5. Yan, F.; Zhao, L.; Patanè, A.; Hu, P.; Wei, X.; Luo, W.; Zhang, D.; Lv, Q.; Feng, Q.; Shen, C.; Chang, K.; Eaves, L.; Wang, K., Fast, multicolor photodetection with graphene-contacted p-GaSe/n-InSe van der Waals heterostructures. *Nanotechnology* **2017**, *28* (27), 27LT01.
6. Pezeshki, A.; Shokouh, S. H. H.; Nazari, T.; Oh, K.; Im, S., Electric and photovoltaic behavior of a few-layer α-$MoTe_2$/MoS_2 dichalcogenide heterojunction. *Advanced Materials* **2016**, *28* (16), 3216-3222.
7. Wu, W.; Zhang, Q.; Zhou, X.; Li, L.; Su, J.; Wang, F.; Zhai, T., Self-powered photovoltaic photodetector established on lateral monolayer MoS_2-WS_2 heterostructures. *Nano Energy* **2018**, *51*, 45-53.
8. Duan, X.; Wang, C.; Shaw, J. C.; Cheng, R.; Chen, Y.; Li, H.; Wu, X.; Tang, Y.; Zhang, Q.; Pan, A.; Jiang, J.; Yu, R.; Huang, Y.; Duan, X., Lateral epitaxial growth of two-dimensional layered semiconductor heterojunctions. *Nature Nanotechnology* **2014**, *9* (12), 1024-1030.
9. Dai, M.; Chen, H.; Feng, R.; Feng, W.; Hu, Y.; Yang, H.; Liu, G.; Chen, X.; Zhang, J.; Xu, C.-Y.; Hu, P., A dual-band multilayer InSe self-powered photodetector with high performance induced by surface plasmon resonance and asymmetric schottky junction. *ACS Nano* **2018**, *12* (8), 8739-8747.
10. Aldalbahi, A.; Rivera, M.; Rahaman, M.; Zhou, A. F.; Mohammed Alzuraiqi, W.; Feng, P., High-performance and self-powered deep UV photodetectors based on high quality 2D boron nitride nanosheets. *Nanomaterials* **2017**, *7* (12).
11. Periyanagounder, D.; Gnanasekar, P.; Varadhan, P.; He, J.-H.; Kulandaivel, J., High performance, self-powered photodetectors based on a graphene/silicon schottky junction diode. *Journal of Materials Chemistry C* **2018**, *6* (35), 9545-9551.
12. Wu, J.; Yang, Z.; Qiu, C.; Zhang, Y.; Wu, Z.; Yang, J.; Lu, Y.; Li, J.; Yang, D.; Hao, R.; Li, E.; Yu, G.; Lin, S., Enhanced performance of a graphene/GaAs self-driven near-infrared photodetector with upconversion nanoparticles. *Nanoscale* **2018**, *10* (17), 8023-8030.
13. Ren, X.; Li, Z.; Huang, Z.; Sang, D.; Qiao, H.; Qi, X.; Li, J.; Zhong, J.; Zhang, H., Environmentally robust black phosphorus nanosheets in solution: application for self-powered photodetector. *Advanced Functional Materials* **2017**, *27* (18), 1606834.
14. Wells, S. A.; Henning, A.; Gish, J. T.; Sangwan, V. K.; Lauhon, L. J.; Hersam, M. C., Suppressing ambient degradation of exfoliated InSe nanosheet devices via seeded atomic layer deposition encapsulation. *Nano Letters* **2018**, *18* (12), 7876-7882.
15. Huang, Z.; Han, W.; Tang, H.; Ren, L.; Chander, D. S.; Qi, X.; Zhang, H., Photoelectrochemical-type sunlight photodetector based on MoS_2/graphene heterostructure. *2D Materials* **2015**, *2* (3), 035011.
16. Qiao, H.; Chen, X.; Wang, B.; Huang, Z.; Qi, X., Novel tin disulfide/graphene photoelectrochemical

photodetector based on solid-state electrolytes and its performances. *Journal of Materials Science: Materials in Electronics* **2019**, *30* (4), 3208-3213.
17. Ren, X.; Qiao, H.; Huang, Z.; Tang, P.; Liu, S.; Luo, S.; Yao, H.; Qi, X.; Zhong, J., Investigating the photocurrent generation and optoelectronic responsivity of WS_2-TiO_2 heterostructure. *Optics Communications* **2018**, *406*, 118-123.